Applied Physics Letters

Growth and structure of $In_{0.5}Ga_{0.5}Sb$ quantum dots on GaP(001)

Cite as: Appl. Phys. Lett. **109**, 102102 (2016); https://doi.org/10.1063/1.4962273
Submitted: 16 February 2016 . Accepted: 19 August 2016 . Published Online: 06 September 2016

E. M. Sala, G. Stracke, S. Selve, T. Niermann, M. Lehmann, S. Schlichting, F. Nippert, G. Callsen, A. Strittmatter, and D. Bimberg

Growth and structure of $In_{0.5}Ga_{0.5}Sb$ quantum dots on GaP(001)

E. M. Sala,[1] G. Stracke,[1] S. Selve,[2] T. Niermann,[3] M. Lehmann,[3] S. Schlichting,[1] F. Nippert,[1] G. Callsen,[1] A. Strittmatter,[1] and D. Bimberg[1,a)]
[1]*Institut für Festkörperphysik, Technische Universität Berlin, Hardenbergstraße 36, 10623 Berlin, Germany*
[2]*Zentraleinrichtung Elektronenmikroskopie, Technische Universität Berlin, Straße des 17. Juni 135, 10623 Berlin, Germany*
[3]*Institut für Optik und Atomare Physik, Technische Universität Berlin, Straße des 17. Juni 135, 10623 Berlin, Germany*

(Received 16 February 2016; accepted 19 August 2016; published online 6 September 2016)

Stranski-Krastanov (SK) growth of $In_{0.5}Ga_{0.5}Sb$ quantum dots (QDs) on GaP(001) by metalorganic vapor phase epitaxy is demonstrated. A thin GaAs interlayer prior to QD deposition enables QD nucleation. The impact of a short Sb-flush before supplying InGaSb is investigated. QD growth gets partially suppressed for GaAs interlayer thicknesses below 6 monolayers. QD densities vary from 5×10^9 to $2 \times 10^{11}\,cm^{-2}$ depending on material deposition and Sb-flush time. When $In_{0.5}Ga_{0.5}Sb$ growth is carried out without Sb-flush, the QD density is generally decreased, and up to 60% larger QDs are obtained. *Published by AIP Publishing*. [http://dx.doi.org/10.1063/1.4962273]

Self-assembled quantum dots (QDs) greatly improve the performance of semiconductor lasers,[1] are suitable for designing easy to fabricate single q-bit emitters,[2] and enable nano-flash memories.[3] By choosing the constituting materials for QDs and surrounding barrier, their electronic configuration can be either type-I (electron- and hole localization) or type-II, spatially indirect.[4,5] Type-II quantum dots showing hole localization are attractive for memory types. A type II discontinuity maximizes the hole localization, as demonstrated by Marent *et al.*[6] who incorporated type II QDs as storage units in a non-volatile nanomemory, the QD-Flash. The QD-Flash shows good endurance and much faster access times (~ns) compared to a conventional Flash memory. In order to operate as a non-volatile memory the storage time for carriers has to be of the order of ten years or longer at room temperature, which depends primarily on the depth of the localization potential and on the capture cross section. As holes possess a larger effective mass than electrons, hole localization in QD-Flash devices is preferred.[7] Thus, QD and matrix material should be chosen to provide a large discontinuity of the valence bands. InGaAs QDs embedded in GaP lead to an increase in the hole storage time by several orders of magnitude as compared to QDs embedded in GaAs.[8,9] Even larger hole localization energies retention times up to years are predicted[10] for InGaSb/GaP QDs. The hole localization energy for $In_{0.5}Ga_{0.5}Sb$/GaAs QDs was calculated to be 919 meV (corresponding to 4 h retention time).[11] By using GaP instead of GaAs another ~700 meV localization depth might be gained,[12] resulting in a carrier localization energy of ~1.6 eV. With this approach, storage times for holes above 10 years are feasible. So far, growth of InGaSb QDs on GaP(001) surfaces has not been demonstrated by metalorganic vapor phase epitaxy (MOVPE), the epitaxial growth method to produce large-scale and therefore cost-effective semiconductor device structures.

In this paper, we demonstrate the growth of $In_{0.5}Ga_{0.5}Sb$ QDs on GaP by MOVPE. It is described as a Stranski-Krastanov growth process,[13] depending strongly on the initial treatment of the GaP surface. All samples were grown in a horizontal Aixtron 200 reactor on the GaP(001) substrates using H_2 as carrier gas. The growth starts with 500 nm GaP grown at 750 °C, upon which temperature is reduced to 500 °C for the following steps comprising: (i) growth of a thin GaAs interlayer, (ii) short Sb-flush, by supply of *triethyl-antimony* (TESb) for one second at input flux of 15.5 μmol/min, and (iii) $In_{0.5}Ga_{0.5}Sb$ growth. The nominal amount of $In_{0.5}Ga_{0.5}Sb$ was assumed to be roughly proportional to that of $In_{0.5}Ga_{0.5}As$ grown at input fluxes of TMGa = 42.5 μmol/min, TMIn = 2.8 μmol/min, and TBA = 7.2 μmol/min. QD ripening process after $In_{0.5}Ga_{0.5}Sb$ deposition was studied through a growth interruption (GRI) series applied without any precursor supply. Structural analysis of QDs is performed *ex-situ* by atomic force microscopy (AFM) and transmission electronic microscopy (TEM).

Deposition of non-lattice matched material leads to SK QD growth by total energy minimization.[13] Size and density of QDs are the functions of the amount of deposited strained material. A significant role in deciding which growth mode prevails is played by surface physics. As reported by us previously for $In_xGa_{1-x}As$/GaP QDs grown by MOVPE,[9,14] the growth of a ~2–3 ML GaAs interlayer prior to the QD deposition is required to enable QD formation. Only two-dimensional InGaAs growth even up to high In contents and comparably large thicknesses (e.g., high lattice stress) could be observed when the interlayer was omitted. A modification of surface energetics for the subsequent growth of InGaAs was achieved by the As-terminated interlayer.

In the present case, the $In_{0.5}Ga_{0.5}Sb$ lattice constant is about ~6.28 Å, according to Vegard's law. The mismatch between GaP and $In_{0.5}Ga_{0.5}Sb$ is 13%, an extremely challenging value for defect-free SK growth and close to enforce Volmer-Weber (VW) island growth mode. As for InGaAs/GaP, neither VW island growth nor SK-QD formation is observed when $In_{0.5}Ga_{0.5}Sb$ was deposited on bare

[a)]Also at King Abdulaziz University, P.O. Box 80200, Jeddah 21589, Kingdom of Saudi Arabia.

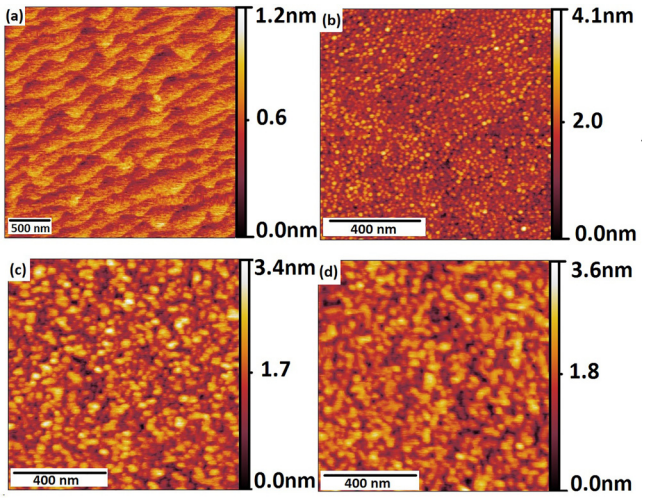

FIG. 1. AFM micrographs of GaP surface after deposition of 0.42 ML $In_{0.5}Ga_{0.5}Sb$: (a) without GaAs layer, with 5 (b), 7 (c), and 8 ML GaAs (d).

GaP. As clearly shown in the AFM micrograph in Fig. 1(a), only monoatomic steps are visible. Using a thin GaAs interlayer enables the QD formation. Since the lattice mismatch between GaAs and GaP is about ~3.5%, two-dimensional growth (Frank-Van der Merwe mode, F-M) of thin GaAs layers on GaP can be maintained. The few layers of GaAs form an As-terminated surface for the following $In_{0.5}Ga_{0.5}Sb$ deposition. However, the mismatch between GaAs and GaP already accumulates strain energy in the layer structure. Subsequent deposition of a sub-monolayer amount of highly mismatched $In_{0.5}Ga_{0.5}Sb$ induces an abrupt change to island growth. 3D islands are already formed after nominal 3 ML GaAs + ~0.21 ML $In_{0.5}Ga_{0.5}Sb$. The strain energy accumulated by the GaAs interlayer contributes to the total energy as can be inferred from the dependence of the QD density on the GaAs interlayer thickness at constant amount of deposited $In_{0.5}Ga_{0.5}Sb$ material. This is shown in Fig. 2 where island density versus GaAs interlayer thickness is plotted for a fixed amount of 0.42 ML $In_{0.5}Ga_{0.5}Sb$. The island density varies from 6×10^9 cm^{-2} for 3 ML GaAs to 2×10^{11} cm^{-2} for 6 ML. If GaAs supply is further increased, small QDs tend to merge to larger ones, as shown in the AFM images in Figs. 1(c) and 1(d) referring to an interlayer thickness of

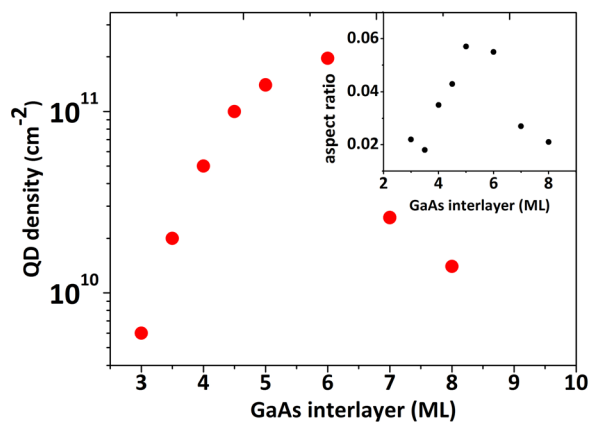

FIG. 2. Variation of QD density versus GaAs interlayer thickness. The inset shows the QD aspect ratio as function of the interlayer. $In_{0.5}Ga_{0.5}Sb$ coverage is kept fixed to 0.42 ML.

7 and 8 ML. The QD density accordingly drops to ~10^{10} cm^{-2}. Here, the QDs show a smaller aspect ratio (height-to-diameter ratio) of ~0.03 compared to those grown on the 5 ML GaAs, showing typically a ratio of ~0.06. The QD heights are between 1.5 and 1.7 (±0.6) nm equal to the values of (1.6 ± 0.5) nm for 0.42 ML $In_{0.5}Ga_{0.5}Sb$ on 5 ML GaAs. Lateral dimensions are increasing however: from (30 ± 5) nm for 5 ML GaAs to (50 ± 12) nm for both 7 and 8 ML GaAs. The observed dependence of QD morphology on the GaAs interlayer thickness indicates incorporation of GaAs into QDs during the QD formation process. The inset of Fig. 2 shows how the QD aspect ratio evolves with increasing interlayer thickness.

To investigate the QD growth mode, we prepared a sample set with increasing $In_{0.5}Ga_{0.5}Sb$ coverage, after deposition of a 5 ML-thick GaAs interlayer and 1s-Sb-flush. The Sb-irradiation prior to $In_{0.5}Ga_{0.5}Sb$ deposition is likely to promote an exchange of Sb atoms for As atoms on the surface[15–17] which can help to increase the Sb content in QDs. Antimony as a large atom may also act as a surfactant, influencing growth generally in many ways,[18–21] modifying, for example, the diffusion length of surface atoms, but also the QD formation.[22–24] On the one hand, an incorporation of small amount of Sb into QDs has been demonstrated for InAs QDs on GaAs.[25] Sun *et al.*[23] also found that less material is needed for 3D island formation, if Sb is irradiated before the QD material deposition. Mazur *et al.*[24] reported more uniform QDs along with higher densities up to ~10^{11} cm^{-2} through the Sb-mediated growth.

The AFM images of free-standing QDs grown on the 5 ML GaAs/GaP are depicted in Fig. 4. From the logarithmic plot in Fig. 4(a), the critical $In_{0.5}Ga_{0.5}Sb$ layer thickness for QD formation is determined to be about 0.21 ML. At this coverage first islands nucleate on the surface, with a density of ~5×10^9 cm^{-2} whereas below this value no QDs can be detected: growth surface for sub-critical InGaSb coverage shows typical monolayer steps of a step-flow growth mode (not shown here). Then, QD density increases exponentially with the amount of deposited $In_{0.5}Ga_{0.5}Sb$ reaching a maximum density of ~2×10^{11} cm^{-2} at 0.6 ML thickness. For more than 1 ML $In_{0.5}Ga_{0.5}Sb$ defect formation is observed (Fig. 3(d)). The observed behavior of the QD formation and evolution is typical of a Stranski-Krastanov growth[26,27] even though a $In_{0.5}Ga_{0.5}Sb$ thickness below 1 ML obviously cannot be referred to a closed layer. As seen earlier, the GaAs interlayer partially contributes to QD formation so that, in the present case, the wetting layer is formed of both interlayer and $In_{0.5}Ga_{0.5}Sb$ material. For an $In_{0.5}Ga_{0.5}Sb$ coverage of 0.42 ML, QD density reaches 1.5×10^{11} cm^{-2} and QDs are on average (30 ± 5) nm wide and (1.6 ± 0.5) nm high, respectively. For $In_{0.5}Ga_{0.5}Sb$ deposition ≥1 ML, an additional nucleation of slightly larger clusters with a density of ~2.5×10^7 cm^{-2} is detected (width of 90 ± 5 nm and height of 5 ± 0.5 nm).

The temporal evolution of 3D islands is studied by applying growth interruptions (GRI) directly after the QD deposition, at the same temperature of 500 °C. During GRI (ranging from 15 s to 60 s), no supplemental precursor for group-V stabilization is provided. Later, the samples were immediately cooled down. In Fig. 4, AFM micrographs of

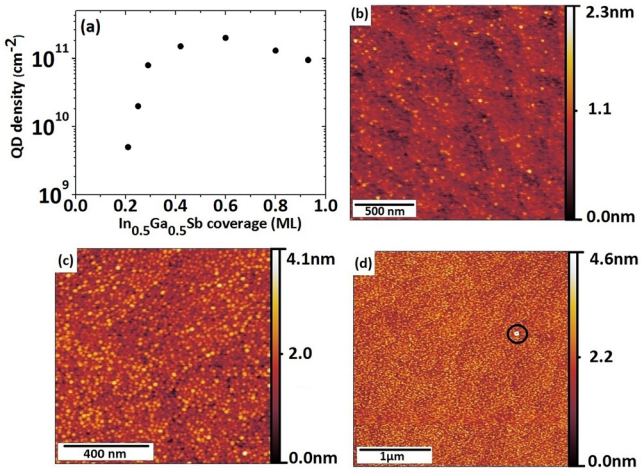

FIG. 3. From left: (a) QD density vs. $In_{0.5}Ga_{0.5}Sb$ coverage. (b)–(d) AFM micrographs of $In_{0.5}Ga_{0.5}Sb$/5 ML GaAs on GaP QDs, using 1 s Sb-flush, with increasing QD material supply: 0.21, 0.42, and 1 ML, respectively. In (d) a cluster is marked by a black circle.

free-standing QDs grown with different GRI durations are shown. Without GRI, QDs have a mean diameter of (40 ± 5) nm and an average height of (1.8 ± 0.5) nm (Fig. 4(a)). The plot in Fig. 4(d) displays the QD density as a function of GRI time: as time increased, larger islands grow and smaller islands disappear, and density is reduced from ∼9.5 × 10^{10} cm^{-2} to ∼2.6 × 10^{10} cm^{-2}. Hence, a ripening process for QDs by material transfer is concluded. Both lateral dimensions and height of QDs increase with time; after 15 s, width and height measure (42 ± 10) nm and (2.3 ± 8) nm, respectively. At 60 s, the mass transfer from small to large islands is particularly evident, where QDs dimensions are of (80 ± 10) nm and (4.5 ± 0.6) nm for width and height, respectively, with a density of ∼1 × 10^{9} cm^{-2}.

In Figs. 5(a)–5(b), cross-sectional TEM micrographs of buried QDs are presented. The sample's [010] zone axis has been tilted away from the electron beam as indicated in the schematic drawing in Fig. 5(a). Thereby, a projected view on the QD growth plane is obtained from which the QD density

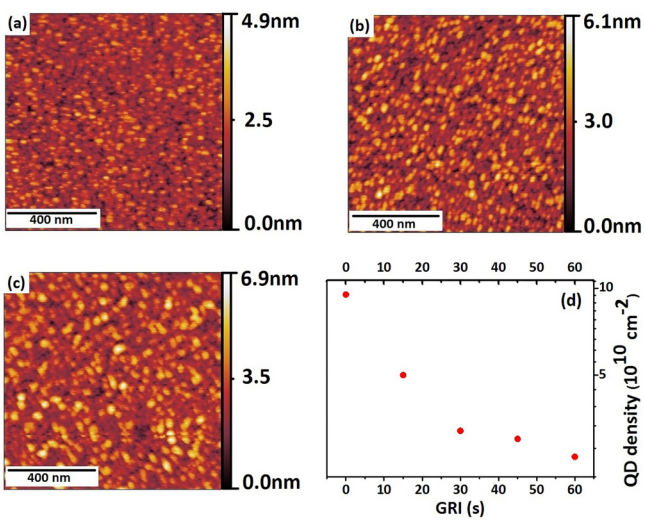

FIG. 4. (a)–(c) AFM measurements of 0.9 ML $In_{0.5}Ga_{0.5}Sb$ QDs/5 ML GaAs/GaP with increasing GRI of 0, 15, and 60 s, respectively. (d) Density trend in respect to time up to 60 s GRI, expressed in seconds.

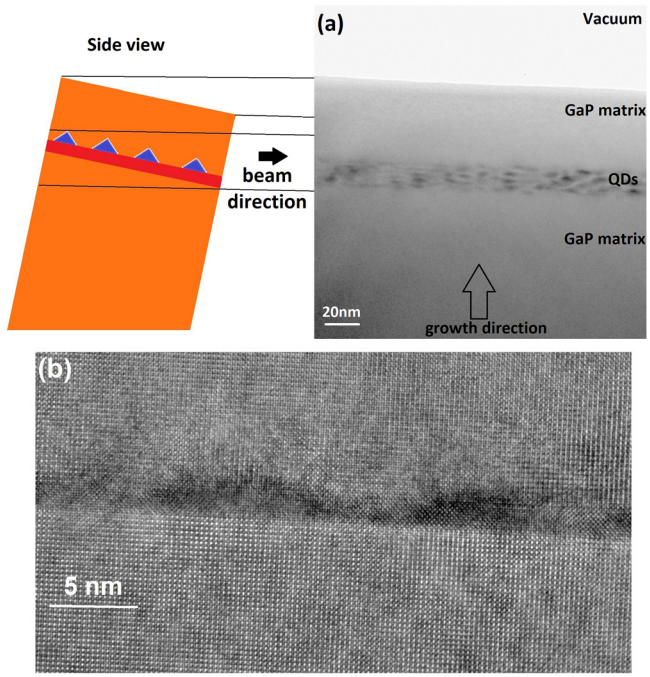

FIG. 5. (a) Cross-sectional TEM images of 0.42 ML $In_{0.5}Ga_{0.5}Sb$ QDs ensemble on 5 ML GaAs/GaP with 1 s Sb-Flush, 15 s GRI, and 6 nm GaP capping layer. The micrographs were taken under strong-beam bright field conditions using the (200) reflection perpendicular to the growth direction. The specimen has been tilted of 6° in respect to the beam direction for visualization of the QD plane: the dark spots represent the QDs. (b) High-resolution micrograph of QDs using the (002) reflection along the [010] zone-axis.

can be deduced. The QDs (dark contrast regions) are distinguishable from the bright background (constituting the GaP matrix) due to a composition contrast. The determination of QD density yields a value of ∼1 × 10^{10} cm^{-2} which is in agreement with the AFM results. A zone-axis high-resolution TEM micrograph of the same QDs is depicted in Fig. 5(b). Dislocation formation during the QD growth can be largely excluded from both images as the diffraction conditions are sensitive to common dislocations in fcc-lattice structures. In Fig. 6, the amplitude signal of a Fourier-filtered (200)-reflection image again taken along the [010]-zone axis of the specimen is shown. The micrograph was obtained in a thinner part of the specimen. Under these conditions, the (200) reflection of the image is primarily linearly imaged, thus the amplitude becomes approximately proportional to the (200)-structure factor of the crystal, which is in

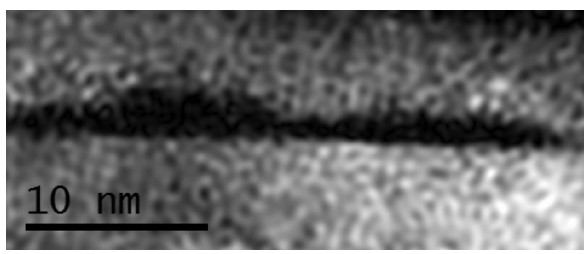

FIG. 6. Amplitude of the Fourier-filtered (200)-reflection of a [010]-zone axis HRTEM image of single 0.42 ML $In_{0.5}Ga_{0.5}Sb$ QDs on 5 ML GaAs/GaP with 15 s GRI and 6 nm GaP capping layer. They were grown without any Sb-Flush. The dark region represents a material contrast whereby the QDs can be easily recognizable.

turn proportional to the difference of the atomic form factors of the species of both fcc-sub-lattices. Hence, this filtered micrograph can be roughly interpreted as concentration map. Here, two single QDs can be clearly detected: they show a truncated-pyramid shape, typical of buried QDs,[28] both with a base length of about 15 nm and a height of 2.5 nm and 1.5 nm, respectively.

In order to investigate the role of antimony-flush on the QD growth, QD deposition was carried out without Sb-flush. The Sb-flush will likely trigger an As-Sb exchange at the surface, leading to GaSb or at least GaAsSb formation. This exchange will therefore increase the total strain in the layer structure prior to the $In_{0.5}Ga_{0.5}Sb$ deposition as compared to bare GaAs interlayers. It is therefore expected to affect the QD density for a given amount of $In_{0.5}Ga_{0.5}Sb$ material. The reference sample set without Sb-flush was grown with the same material supply as before and the GaAs interlayer thickness was kept at 5 ML. Without Sb-flush, larger QDs with densities reduced by a factor of 2 to 7 are formed (not shown here). Otherwise, no changes in the previously observed general trends are found. It turns out that higher QD densities can be achieved with Sb-flush as compared to samples without the Sb-flush because of a decreased tendency for defect formation at long $In_{0.5}Ga_{0.5}Sb$ QD deposition times.

The optical properties of the $In_{0.5}Ga_{0.5}Sb$/GaAs/GaP QDs are investigated by temperature-dependent (PL) and time-resolved photoluminescence (TRPL). PL was recorded using a 445 nm laser diode with 500 mW output power for excitation. For TRPL experiments, a setup comprising a dye laser system delivering ns-pulses at 445 nm was used along with a detection system having a resolution of ~0.5 ns. Fig. 7 shows the static PL measurements of three different samples. Luminescence of samples containing only the GaAs intermediate layer is detected at 1.88 eV. The substructures arising on both the low and high energy sides of it might come from island formation at the two interfaces of this thin

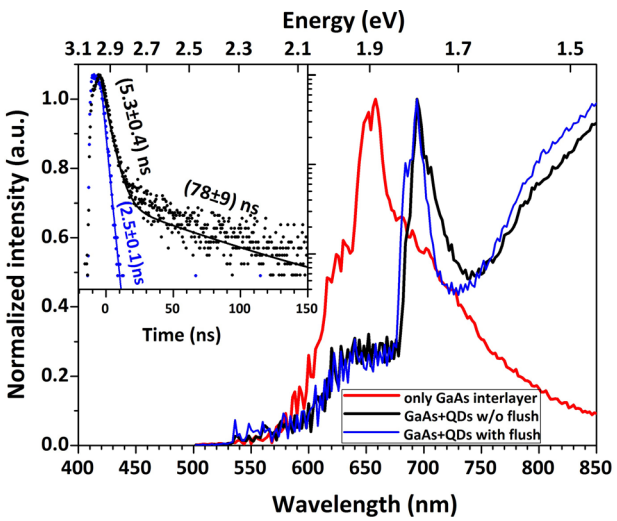

FIG. 7. PL spectra at 10 K of $In_{0.5}Ga_{0.5}Sb$ QDs on 5 ML GaAs/GaP: (blue) with Sb-flush; (black) without Sb-flush; (red) no QDs, only 5 ML GaAs/GaP; normalized to 1.0. Inset: Time-resolved PL transients (at 4 K) recorded at 695 nm emission wavelengths for $In_{0.5}Ga_{0.5}Sb$ QDs grown with (blue) and without (black) Sb-flush. Solid lines show mono- or bi-exponential fits to the data.

QW, being only a few MLs thick.[29] Upon $In_{0.5}Ga_{0.5}Sb$ supply, the 1.88 eV transition is still present, although with lower intensity, and a new lower energy transition at 1.78 eV is found, attributed to QDs. The temperature dependence of this emission line exhibits clear signatures of carrier localization between 10 K and 100 K, typical for QDs (not shown here). A thermalization process of originally localized carriers in the lowest energy QDs occurs between 50 K and 80 K leading to a blue-shift in emission energy. In contrast, luminescence from the GaAs interlayer follows the well-known Varshni behavior. The TRPL measurements of the emission line at 1.78 eV for the two QD structures were taken. The inset of Fig. 7 shows the existence of two different recombination processes in samples with and without the Sb-flush. Without the Sb-flush, TRPL exhibits a fast initial component ($\tau_{life} = 5.3$ ns), followed by a slower decay ($\tau_{life} = 78$ ns). Such behavior is typical for QDs with type-II band alignment as discussed by Hatami *et al.*[30,31] Decay time constants around 5 ns were reported[31] at larger excitation densities, very similar to our present initial decay times ($\tau_{d1} = 5.3$ ns). The decay times at lower carrier densities ($\tau_{d2} = 78$ ns) are longer here and become closer to what one naively expects for type II QDs. In contrast, the TRPL of the sample with Sb-flush exhibits only a fast decay component ($\tau_{life} = 2.5$ ns). Apparently, Sb-flush prior to the QD deposition leads to a type I transition again similar to the previous observation.[31]

In conclusion, we have demonstrated SK growth of $In_{0.5}Ga_{0.5}Sb$ QDs on GaP in a MOVPE environment. QD nucleation has been achieved by growing a thin GaAs interlayer prior to $In_{0.5}Ga_{0.5}Sb$ deposition. The QD density changes both with the amount of $In_{0.5}Ga_{0.5}Sb$ as well as with the GaAs interlayer thickness, suggesting a heterogeneous, intermixed material to be involved in the 2D/3D transition; QD densities in a range of $\sim 5 \times 10^9$ to $\sim 2 \times 10^{11}$ cm^2 could be realized. An island ripening is deduced from the evolution of QD size and density during growth interruptions. The kinetics of QD growth are better controllable and higher QD densities can be achieved upon short Sb-irradiation of the GaAs interlayer surface. The Sb-flush, however, leads to a much faster temporal decay behavior, indicating a type I transition.

The authors thank the DFG (Contract No. BI284/29-2), the Federal Ministry of Economics and Technology (BMWi), Grant No. 03VWP0059v, and the Federal Ministry of Education and Research (BMBF), Grant No. 16V0196 (HOFUS).

[1]D. Bimberg, Electron. Lett. **44**, 168 (2008).
[2]W. Unrau and D. Bimberg, Laser Photonics Rev. **8**, 276 (2014).
[3]M. Geller, A. Marent, and D. Bimberg, in *Handbook of Nanophysics: Nanoelectronics and Naophotonics*, edited by K. D. Sattler (CRC Press, Boca Raton, FL, 2010), Sect. 2.1.
[4]I. Vurgaftman, J. R. Meyer, and L. R. Ram-Mohan, J. Appl. Phys. **89**, 5815 (2001).
[5]J. He, C. J. Reyner, B. L. Liang, K. Nunna, D. L. Huffaker, N. Pavarelli, K. Gradkowski, T. J. Ochalski, G. Huyet, V. G. Dorogan, Yu. I. Mazur, and G. J. Salamo, Nano Lett. **10**, 3052–3056 (2010).
[6]A. Marent, M. Geller, and D. Bimberg, Microelectron. J. **40**, 492–495 (2009).

[7]A. Marent, T. Nowozin, J. Gelze, F. Luckert, and D. Bimberg, Appl. Phys. Lett. **95**, 242114 (2009).
[8]G. Stracke, A. Glacki, T. Nowozin, L. Bonato, S. Rodt, C. Prohl, A. Lenz, H. Eisele, A. Schliwa, A. Strittmatter, U. W. Pohl, and D. Bimberg, Appl. Phys. Lett. **101**, 223110 (2012).
[9]L. Bonato, E. M. Sala, G. Stracke, T. Nowozin, A. Strittmatter, M. N. Ajour, K. Daqrouq, and D. Bimberg, Appl. Phys. Lett. **106**, 042102 (2015).
[10]T. Nowozin, D. Bimberg, K. Daqrouq, M. N. Ajour, and M. Awedh, J. Nanomater. **2013**, 215613.
[11]A. Marent, M. Geller, A. Schliwa, D. Feise, K. Pötschke, D. Bimberg, N. Akçay, and N. Öncan, Appl. Phys. Lett. **91**, 242109 (2007).
[12]M. Di Ventra, M. Peressi, and A. Baldereschi, Phys. Rev. B **54**, 5691–5695 (1996).
[13]V. A. Shchukin, N. N. Ledentsov, P. S. Kopev, and D. Bimberg, Phys. Rev. Lett. **75**, 2968–2971 (1995).
[14]G. Stracke, E. M. Sala, S. Selve, T. Niermann, A. Schliwa, A. Strittmatter, and D. Bimberg, Appl. Phys. Lett. **104**, 123107 (2014).
[15]Y. Q. Wang, Z. L. Wang, T. Brown, A. Brown, and G. May, J. Cryst. Growth **242**, 5–14 (2002).
[16]H. Eisele and M. Dähne, J. Cryst. Growth **338**, 103–106 (2012).
[17]I. Farrera, M. J. Murphy, D. A. Ritchie, and A. J. Shield, J. Cryst. Growth **251**, 771–776 (2003).
[18]R. Wixom, N. Modine, and G. Stringfellow, Phys. Rev. B **67**, 115309 (2003).
[19]J. Zhu, F. Liu, and G. B. Stringfellow, J. Cryst. Growth **312**, 174–179 (2010).
[20]G. Rosenfeld, R. Servaty, C. Teichert, B. Poelsema, and G. Comsa, Phys. Rev. Lett. **71**, 895–898 (1993).
[21]C. S. Peng, Q. Huang, W. Q. Cheng, J. M. Zhou, Y. H. Zhang, T. T. Sheng, and C. H. Tung, Appl. Phys. Lett. **72**, 2541–2543 (1998).
[22]D. Guimard, M. Nishioka, S. Tsukamoto, and Y. Arakawa, J. Cryst. Growth **298**, 548–552 (2007).
[23]Y. Sun, S. F. Cheng, G. Chen, R. L. Woo, and R. F. Hicks, J. Appl. Phys. **97**, 053503 (2005).
[24]Yu. I. Mazur, V. G. Dorogan, G. J. Salamo, G. G. Tarasov, B. L. Liang, C. J. Reyner, K. Nunna, and D. L. Huffaker, Appl. Phys. Lett. **100**, 33102 (2012).
[25]D. Guimard, S. Tsukamoto, M. Nishioka, and Y. Arakawa, Appl. Phys. Lett. **89**, 083116 (2006).
[26]I. N. Stranski and L. Krastanow, Monatshefte Chem. **71**, 351 (1937).
[27]D. Leonard, K. Pond, and P. M. Petroff, Phys. Rev. B **50**, 11687 (1994).
[28]A. Lenz, R. Timm, H. Eisele, C. Hennig, S. K. Becker, R. L. Sellin, U. W. Pohl, D. Bimberg, and M. Dähne, Appl. Phys. Lett. **81**, 5150 (2002).
[29]M. A. Herman, D. Bimberg, and J. Christen, J. Appl. Phys. **70**, R1 (1991).
[30]F. Hatami, N. N. Ledentsov, M. Grundmann, J. Böhrer, F. Heinrichsdorff, M. Beer, D. Bimberg, S. S. Ruvimov, P. Werner, U. Gösele, J. Heydenreich, U. Richter, S. V. Ivanov, B. Ya. Meltser, P. S. Kop'ev, and Zh. I. Alferov, Appl. Phys. Lett. **67**, 656 (1995).
[31]F. Hatami, M. Grundmann, N. N. Ledentsov, F. Heinrichsdorff, R. Heitz, J. Böhrer, D. Bimberg, S. S. Ruvimov, P. Werner, V. M. Ustinov, P. S. Kop'ev, and Zh. I. Alferov, Phys. Rev. B **57**, 4635 (1998).